Available online at www.sciencedirect.com
SCIENCE DIRECT
Tectonophysics 421 (2006) 111–127
TECTONOPHYSICS
www.elsevier.com/locate/tecto

Petrofabrics and seismic properties of garnet peridotite from the UHP Sulu terrane (China): Implications for olivine deformation mechanism in a cold and dry subducting continental slab

Zhiqin Xu [a], Qin Wang [b], Shaocheng Ji [c], Jing Chen [d], Lingsen Zeng [a,*], Jingsui Yang [a], Fangyuan Chen [a], Fenghua Liang [a], Hans-Rudolf Wenk [e]

[a] *Key Laboratory of Continental Dynamics, Ministry of Land and Resources. Institute of Geology, Chinese Academy of Geological Sciences, Beijing 100037, China*
[b] *Department of Earth Sciences, Nanjing University, Nanjing 210093, China*
[c] *Département des Génies Civil, Géologique et des Mines, École Polytechnique de Montréal, Montréal, Québec, Canada H3C 3A7*
[d] *Institute of Physics, Beijing University, Beijing 100871, China*
[e] *Department of Geology and Geophysics, University of California, Berkeley, CA 94720, USA*

Received 16 January 2006; received in revised form 2 April 2006; accepted 16 April 2006

Abstract

Lattice-preferred orientations (LPO) of olivine, diopside, enstatite and garnet from the Zhimafang garnet peridotite body in the Sulu ultrahigh-pressure (UHP) metamorphic terrane (China) were measured using the electron backscatter diffraction (EBSD) technique. The peridotite was captured from a mantle wedge immediately adjacent the subducted Yangtze slab and then experienced the UHP metamorphism at 750–950 °C and 4–7 GPa. The olivine LPO is characterized by the [001] axis close to the stretching lineation and the (100) plane subparallel to the foliation, indicating the prevailing of (100) [001] slip. Enstatite LPO displays the dominance of (100) [001] slip. Diopside developed complex LPO patterns that are difficult to explain using a single slip system of (100) [001]. Garnet is almost randomly oriented due to its low volume fractions, cubic symmetry and the presence of numerous slip systems. Calculated seismic properties of the peridotite yield a maximum P-wave velocity normal to the foliation and a minimum along the foliation, with anisotropy up to 8% in strongly sheared samples. The S-wave velocity pattern is complex but the fast polarization plane generally normal to the foliation. The inferred shear sense from the olivine LPO is top-to-SE, in contrary to exhumation-induced top-to-NW thrusting recorded in the quartz LPO, implying that the olivine LPO formed at early UHP metamorphic conditions. The olivine crystals have relatively low water contents (141–475 H/10^6 Si), indicating a fluid-deficient environment for the LPO formation. The present study suggests that a combination of low temperature and UHP plays a much more important role than the water content to promote the activation of (100) [001] slip in olivine.

Keywords: Olivine; Lattice-preferred orientation; Water content; Subducted continental slab; Ultrahigh-pressure metamorphism; Sulu terrane

1. Introduction

Seismic anisotropy of the upper mantle is generally attributed to the lattice-preferred orientation (LPO) of olivine, which results from dislocation slip in response

* Corresponding author. Tel.: +86 10 68992975; fax: +86 10 68994782.
E-mail address: lzeng@ccsd.org.cn (L. Zeng).

0040-1951/$ - see front matter © 2006 Elsevier B.V. All rights reserved.
doi:10.1016/j.tecto.2006.04.010

to plastic flow (e.g., Mercier, 1985; Nicolas and Christensen, 1987). Carter and Avé Lallemant (1970) found that as temperature rises, the dominant slip system in olivine changes sequentially from (100) [001], then {110} [001], {0*kl*} [100], and finally to (010) [100]. The dominant activation of (010) [100] slip system produces parallelisms of olivine [100] axis and (010) plane with the shear direction and plane, respectively. Because the [100] is the crystallographic direction of maximum P-wave velocity and [010] is the minimum in olivine, the fastest P-wave velocity of peridotite is nearly parallel to the stretching lineation and the polarization plane of the fastest S-wave to the foliation plane (e.g., Mainprice and Silver, 1993; Ji et al., 1994; Wenk and Tomé, 1999; Tommasi et al., 2000). So far this relationship has been widely used to trace the mantle flow from seismic anisotropy observations (e.g., Savage, 1999; Park and Levin, 2002).

Recently much attention has been paid to the activation of other slip systems than (010) [100] in olivine as functions of physicochemical conditions such as temperature, pressure and water content, and to the induced seismic anisotropy in the upper mantle. Jung and Karato (2001) reported that water could enhance the slip along the [001] direction and result in a dominant (100) [001] slip system at modest stress in wet olivine. If this is true, the occurrence of (100) [001] olivine fabrics can be used as an indicator of high water content in the upper mantle (e.g., Frese et al., 2003; Mizukami et al., 2004; Katayama et al., 2005). However, the [001] glide on (100) or (010) plane can also develop in water-poor olivine under high-pressure conditions (Li et al., 1999; Couvy et al., 2004; Raterron et al., 2004). Using a viscoplastic self-consistent model, Mainprice et al. (2005) simulated development of olivine LPO at high pressure and found [001] slip system is significantly easier than [100] systems. They used the results to explain the rapid decrease of anisotropy below 250 km in the upper mantle.

Most olivine LPO data published in the literature are measured from ophiolites and xenoliths (e.g., Nicolas and Christensen, 1987; Ji et al., 1994; Ben Ismaïl and Mainprice, 1998; Saruwatari et al., 2001). However, few data are from ultrahigh-pressure (UHP) metamorphic terranes in which garnet peridotites are one of the most important components (Medaris, 1999; Brueckner and Medaris, 2000; Liou et al., 2000b). These garnet peridotites generally occur as boudins in coesite-bearing quartzo-feldspathic gneisses and mafic eclogites, and are believed to come from the mantle wedge immediately above the subducted continental lithosphere, and both were exhumed to the Earth's surface by the same tectonic process. Here we report our research results on LPOs and seismic properties of the Zhimafang garnet peridotite in the UHP Sulu terrane, eastern China. This garnet peridotite, which experienced UHP (4–7 GPa), low temperature (750–950 °C) and relatively low water content (<500 H/10^6 Si) peak metamorphism, developed typical (100) [001] olivine fabrics. The results suggest that a combination of low temperature and UHP plays a more important role than water content to promote the (100) [001] slip in olivine. The calculated seismic properties of the UHP peridotite are also helpful to interpret seismic anisotropy within a cold and relatively dry subducted slab and in the adjacent upper mantle.

2. Geological setting

As the largest recognized UHP terrane in the world, the Dabie–Sulu orogenic belt was formed by the Triassic collision between the North China and Yangtze plates (e.g., Li et al., 1999; Hacker et al., 2000). Presence of coesite, microdiamond and other UHP mineral assemblages in eclogite, pelitic and granitic gneisses, quartzite and marble demonstrates that the continental crust of the Yangtze plate was subducted to mantle depths >150 km (e.g., Liou et al., 1998; Ye et al., 2000; Liu et al., 2001, 2002). SHRIMP U–Pb dating suggests that a peak UHP event occurred in the Sulu terrane at 231±4 Ma, closely followed by the amphibolite–facies retrograde metamorphism at 211±4 Ma (Liu et al., 2004).

The Sulu terrane, which is bounded by the Qingdao–Wulian fault in the north and the Jiashan–Xiangshui fault in the south, was northward displaced about 530 km from the Dabie terrane by the Tan-Lu fault. From south to north, the Sulu terrane can be divided into four units: (1) Low temperature and high pressure (LT/HP: T=300–360 °C and P=0.7–0.85 GPa, Qiu et al., 2002) gneisses and greenschists characterized by the occurrence of glaucophane, phengite and aragonite; (2) Medium temperature (MT) and very high pressure (VHP) kyanite-bearing quartzite and marble (T=500–600 °C and P=1.5–2.0 GPa, Zhang et al., 2002); (3) Southern UHP supracrustal rocks; and (4) Northern UHP granitic rocks (Fig. 1a). The SE–SSE dipping foliation and SE-plunging lineation dominate in the south, while the NW–NWW dipping foliation and NW-plunging lineation develop in the north Sulu terrane, indicating a regional top-to-NW thrusting along a major dome-shaped shear zone during exhumation (Faure et al., 2003; Xu et al., 2003b). In addition, NS-streching

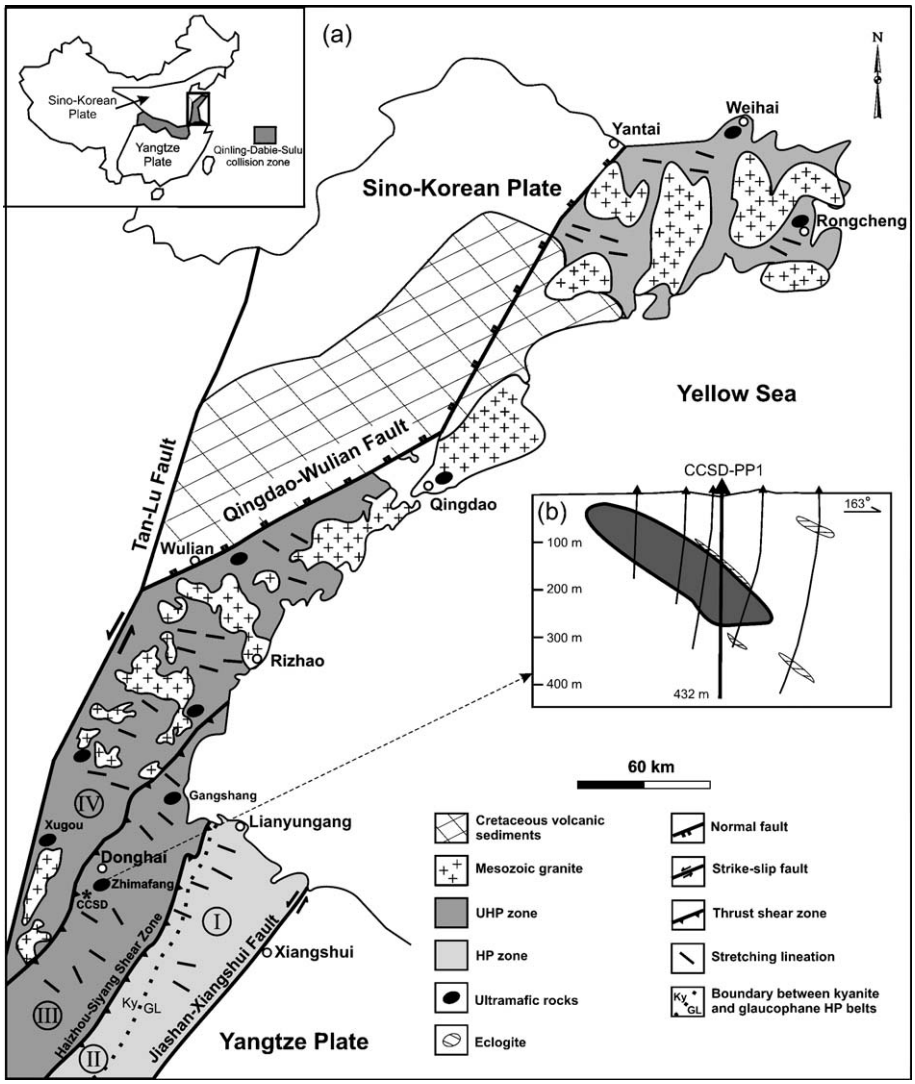

Fig. 1. (a) Simplified geological map of the Sulu terrane, eastern China, showing distribution of ultramafic rocks in the Sulu UHP zone. Tectonic units of the Sulu terrane: I, LT/HP glaucophane zone; II, MT/VHP kyanite zone; III, south UHP supracrustal zone; IV, north UHP granitic zone (modified after Xu et al., 2003a,b). (b) Cross-section of the Zhimafang garnet peridotite (from the No. 6 Geological Team of Jiangsu Province).

lineation, which is related to the early northward subduction of the Yangtze plate (Xu et al., 2003b), has been found in the Sulu UHP zone and the LT/HP belt. Although less than 5 vol.% at the surface, ultramafic rocks and eclogite widely spread in the Sulu UHP zone. Garnet peridotites occur as lenses, pods and layers ranging from tens of centimetres to a few kilometres in size within foliated eclogite and felsic gneiss. The peak metamorphic conditions of garnet peridotites reach 750–950 °C and 4–7 GPa, implying an extremely low geothermal gradient (≤5 °C/km) in the subducted continental slab (Zhang et al., 1994, 2003; Liou et al., 2000a).

The Zhimafang garnet peridotite body, 970-m-long and 170-m-wide, is located about 9 km SE of Donghai County (Fig. 1a). The No. 6 geological team of Jiangsu Province drilled 11 shallow boreholes into the ultramafic body and its surrounding supracrustal gneisses and eclogite lenses (Fig. 1b). Separated from the quartzo-feldspathic gneisses by faults, the Zhimafang peridotite developed a SE-dipping foliation and a SE-plunging lineation. The lineation is defined by shape preferred orientations of olivine, orthopyroxene, clinopyroxene and spinel. A 432.08-m-deep pre-pilot hole (CCSD-PP1) of the Chinese Continental Scientific Drilling project at N34°30′ and E118°47′

penetrated granitic gneiss, paragneiss, eclogite and peridotite. The thickness of peridotite in the CCSD-PP1 reaches 118 m, including a fresh to slightly serpentinized middle part (155.15–238.51 m), and strongly serpentinized and chloritized top (138–155.15 m) and bottom (238.51–256 m) parts (Liu et al., 2001). Except dunite, harzburgite, wehrlite and lherzolite generally contain garnet porphyroclasts with sizes ranging from 1 to 5 mm. The compositional change from garnet-bearing peridotite to garnet-free dunite is transitional.

Unlike its adjacent felsic gneisses and eclogite that contain coesite-bearing zircons, the Zhimafang garnet peridotite contains UHP mineral assemblages and exsolution textures (Yang et al., 1993; Zhang et al., 1994; Yang and Jahn, 2000; Xu et al., 2003a). The presence of these characteristic minerals indicates that the peridotite together with its country rocks have experienced a coeval UHP metamorphism. U–Pb SHRIMP geochronology of zircon suggests that the UHP metamorphism occurred at 221±3 Ma (Zhang et al., 2005). Furthermore, the Zhimafang peridotite contains lower fertile element concentrations than the primitive mantle and shows negative correlations between MgO content versus Al_2O_3, CaO and TiO_2, implying an origin as depleted residual mantle materials (Zhang et al., 2000; Li et al., 2003a,b).

3. Petrography and microstructure

Table 1 gives the sampling depth and major oxide contents of garnet peridotite from the CCSD-PP1. With granular to semi-tabular texture, sample 141-12 is a slightly altered garnet wehrlite containing about 60% olivine, 30% diopside and 5% garnet. Samples 144-9, and 150-4 (Fig. 2a) are fresh, weakly deformed garnet lherzolites composed of about 45% olivine, 40% diopside, 10% enstatite, 2–5% garnet, and minor phlogopite and spinel. Olivine generally occurs as fractured, rounded grains and contains abundant exsolution lamellae of ilmenite. Diopside and enstatite appear as prismatic crystals and occasionally contain exsolution of oriented ilmenite, phlogopite and chromite. Garnet is anhedral in size of 1–10 mm and contains aligned diopside and enstatite inclusions (Fig. 2d).

Sample 151-11 (Fig. 2b) is a foliated garnet lherzolite with ~10 vol.% phlogopite and large porphyroclastic garnet (up to 20 mm). The aspect ratios of olivine and diopside are 3–4 : 1. Phlogopite developed two generations: euhedral phlogopite equilibrated with the primary phases, and chloritized anhedral platelets in the tail of garnet pressure shadows. Sample 160-9 is a strongly foliated and partially serpentinized lherzolite consisting of olivine, diopside, minor enstatite, garnet as well as phlogopite (Fig. 2c). The aspect ratios of elongated olivine grains are up to 10:1. Many olivine crystals are relics in a network of serpentine. With semi-tabular texture, sample 166-7 is a phlogopite-rich lherzolite, containing well-preserved grains of olivine and diopside, abundant secondary phlogopite and minor garnet and spinel.

4. EBSD measurements

The LPOs of olivine, diopside, enstatite and garnet were measured using a scanning electron microscope

Table 1
Sampling depths and chemical compositions (wt.%) of the core samples from the pre-pilot borehole CCSD-PP1

Sample no.	141-12	144-9	150-4	151-11	160-9	166-7
Lithology	Grt wehrlite	Grt lherzolite	Grt lherzolite	Grt lherzolite	Srp lherzolite	Phl lherzolite
Depth (m)	151.74	157	178.1	180.5	210.35	224.96
SiO_2	40.54	42.71	43.09	42.03	43.45	42.78
TiO_2	0.02	0.01	0.00	0.02	0.01	0.01
Al_2O_3	3.59	1.91	1.12	1.41	2	1.53
Cr_2O_3	0.41	0.40	0.40	0.4	0.3	0.44
TFeO	7.82	7.44	7.67	8.37	7.42	7.59
MnO	0.13	0.11	0.11	0.11	0.1	0.11
MgO	37.32	43.92	44.42	44.28	41.32	44.13
CaO	2.48	1.02	0.56	1.1	1.65	0.67
Na_2O	0.14	0.06	0.07	0.07	0.13	0.06
K_2O	0.08	0.23	0.05	0.02	0.13	0.18
P_2O_5	<0.10	<0.10	<0.10	<0.10	<0.10	<0.10
NiO	0.24	0.28	0.26	0.25	0.24	0.26
LOI	7.86	2.70	1.98	1.96	3.78	2.72
Total	100.6	100.79	99.73	100.02	100.53	100.48

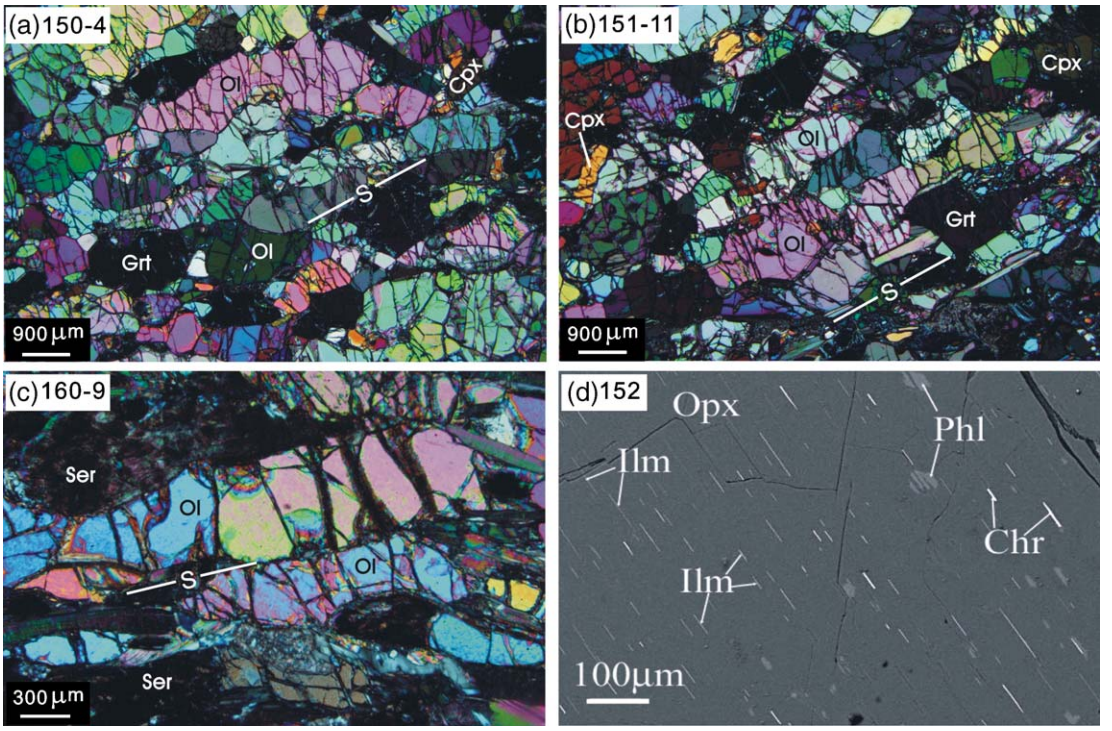

Fig. 2. Photomicrographs showing mineral assemblages and texture of the Zhimafang garnet peridotite: (a) 150-4, (b) 151-11, (c) 160-9, (d) 152. Thin sections cut parallel to the *XZ* plane. Cross polarizers. Foliation indicated by S. Mineral abbreviations: Grt – garnet, Ol – olivine, Cpx – clinopyroxene, Opx – orthopyroxene, Ser – serpentine, Ilm – ilmenite, Chr – chromite, Phl – phlogopite.

JEOL JSM-5610LV by electron backscatter diffraction (EBSD) technique. Thin sections were cut parallel to the structural *XZ*-plane (*X* – parallel to the lineation, *Y* – parallel to foliation and normal to lineation, *Z* – normal to foliation) and carefully polished, then were put in the microscope chamber with 70° tilt angle. The electron backscatter patterns were acquired at accelerating voltage of 20 kV and a working distance of 20 mm. The photonic images were indexed by the CHANNEL5 software. For all the samples, the whole surface was analyzed in automatic procedure with a step size of 50 μm in *x* and *y* directions. Discriminators were used to reject suspicious indexing. Although the step size cannot avoid duplicate measurements in big grains, it provides statistically reliable results. The relative precision of crystal orientations measured from electron backscatter patterns is better than 1° (Krieger Lassen, 1996). Pole figures of the three crystallographic axes and calculated seismic properties of peridotite were contoured using the software of Mainprice (1990, 2005).

Fig. 3 shows the EBSD-measured LPO of olivine from the six core samples. For samples 150-4, 151-11, 160-9 and 166-7, the maximum concentration of [001] axes is nearly parallel to the lineation and a partial girdle of the [100] axes is normal to the foliation. The fabric pattern indicates that (100) [001] slip system was predominantly active in these strongly deformed samples. However, the olivine LPOs in weakly deformed samples 141-12 and 144-9 are relatively complex. For sample 166-7, a dextral shear sense is inferred from the fabric obliquity with respect to the structural foliation and lineation, reflecting a top-to-SE shear event. The angle between the maximum concentrations of [001] axes to the lineation is 24°–35° on a Wulff net. The pfJ index describes the sharpness of a pole figure and increases with the fabric strength. It is less than 2.0 in samples 141-12, 144-9 and 150-4, and reaches 5.5 in sample 160-9, implying strain localization between 180 m and 224 m in the borehole CCSD-PP1.

Enstatite in garnet lherzolite 144-9, 150-4 and 151-11 shows an asymmetric LPO pattern with the maximum of [001]-axes subparallel to the lineation and the [100]-axes subnormal to the foliation (Fig. 4). This pattern can be easily explained by the dominant slip of (100) [001] system. However, the inferred shear sense is sinistral for sample 150-4 and dextral

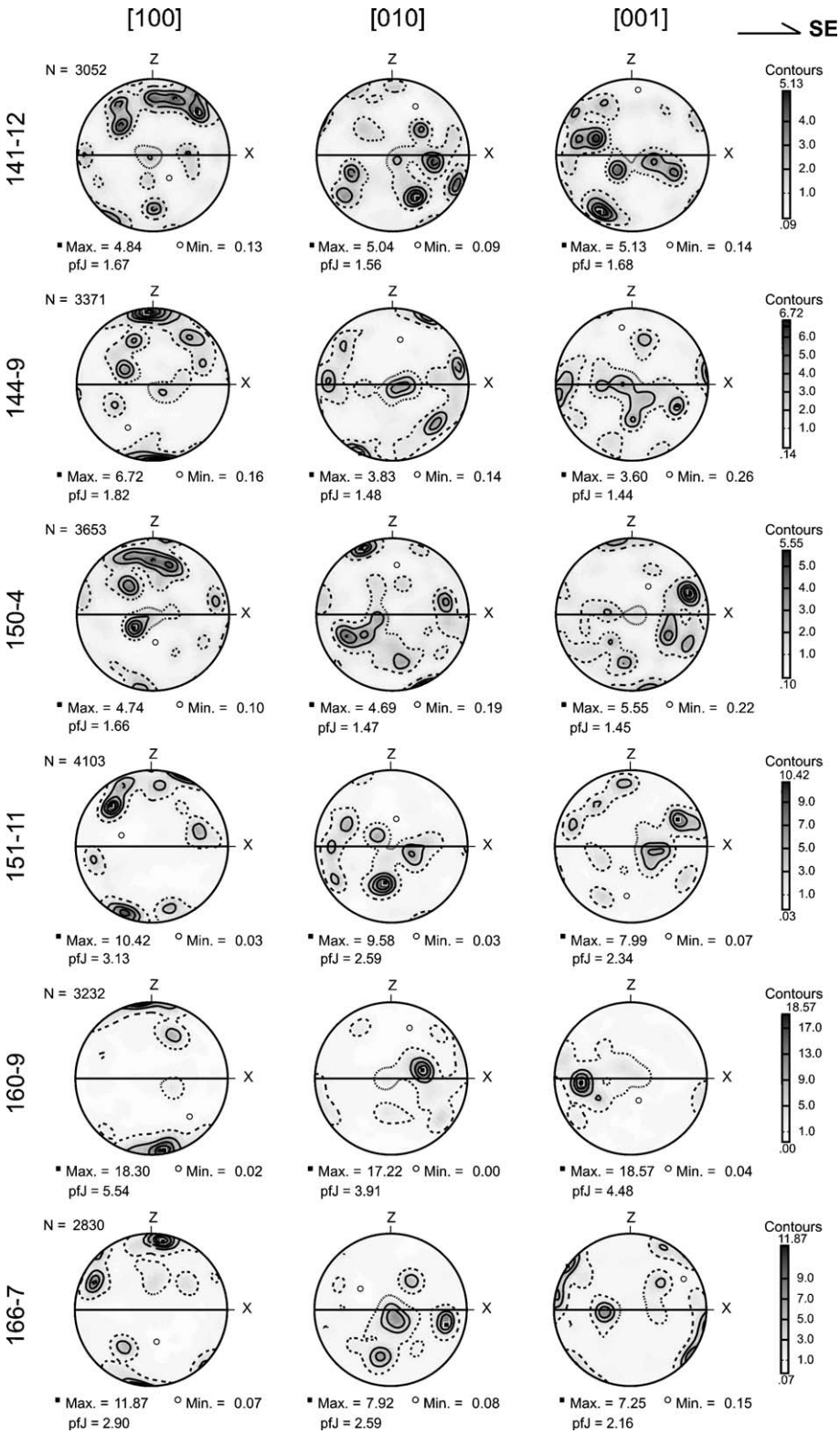

Fig. 3. EBSD-measured lattice preferred orientations of olivine from the Zhimafang garnet peridotite. Equal area projection, lower hemisphere. The contours at multiples of a uniform distribution are plotted and an inverse log grey scale is used to emphasize high densities. Structural directions *X*, *Y* and *Z* are defined in the text. *N*: number of data points; pfJ: texture index.

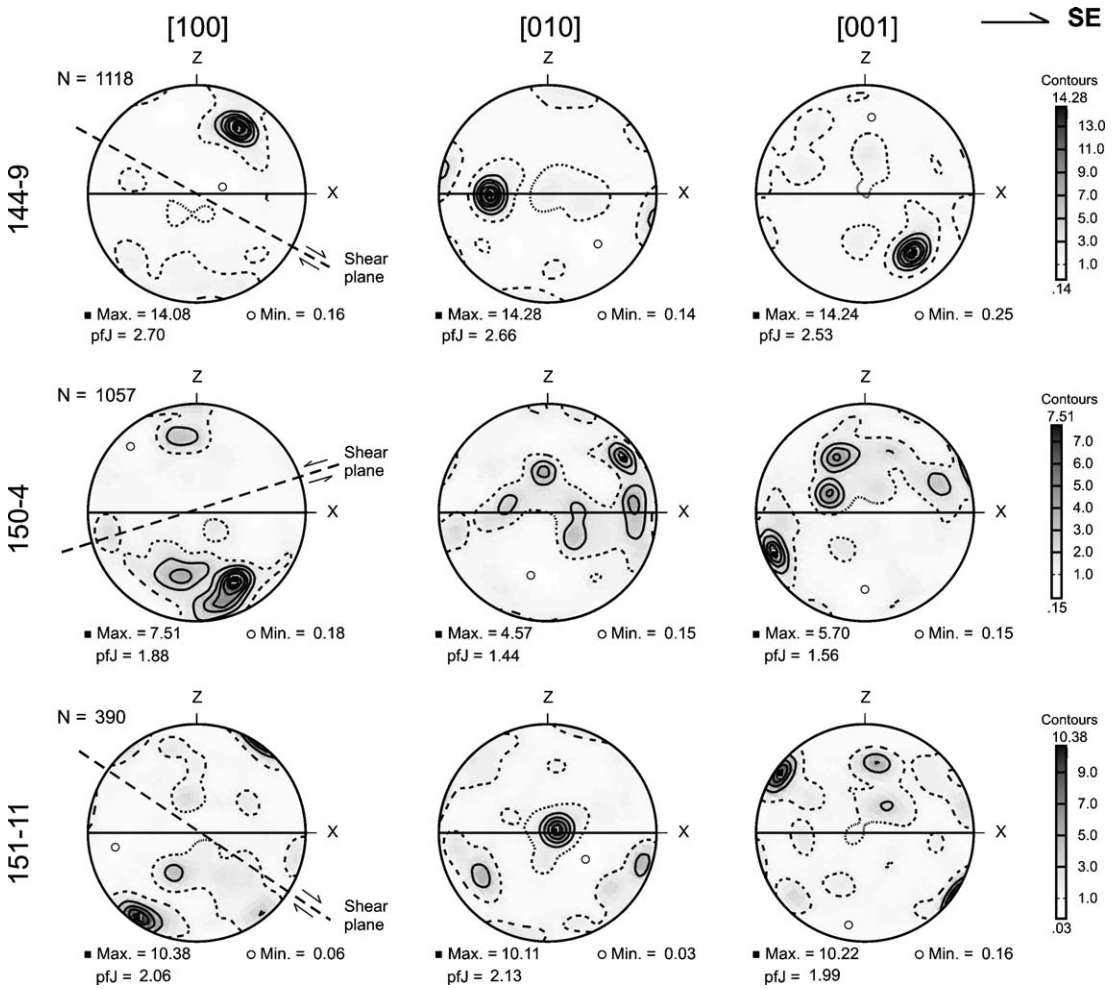

Fig. 4. EBSD-measured enstatite LPO from the Zhimafang garnet lherzolite. Equal area projection, lower hemisphere, contouring as multiples of a uniform distribution and an inverse log grey scale. Structural directions *X*, *Y* and *Z* are defined in the text. *N*: number of data points; pfJ: texture index. The dashed line represents inferred shear plane from the enstatite fabrics.

for samples 144-9 and 151-11, reflecting a complex and heterogeneous flow in the garnet peridotite. The LPOs of diopside are relatively weak and show complex patterns (Fig. 5). However, sample 160-9 is distinguishable by the strong concentration of diopside (010)-poles subparallel to *Y* and [001]-axes subnormal to the foliation. The garnet LPO is very weak (Fig. 6), which is attributed to its low volume fraction in the rocks and cubic symmetry and 66 possible slip systems (Ji et al., 2003a,b; Mainprice et al., 2004).

5. Calculated seismic properties

Ignoring the contribution of phlogopite and other alteration minerals, seismic properties of the Zhimafang garnet peridotite are calculated from EBSD-measured LPOs of major minerals and re-adjusted modal compositions using Hill average (Table 2). The single crystal elastic constants and density data are from studies on olivine (Abramson et al., 1997), diopside (Collins and Brown, 1998), enstatite (Chai et al., 1997a), and pyrope (Chai et al., 1997b).

The seismic properties of studied garnet peridotites are summarized in Table 3. Fig. 7 presents 3D results in equal area projection of lower hemisphere. The fast P-wave velocities range from 8.40 km/s to 8.73 km/s with the propagation direction normal to the foliation. P- and S-wave anisotropy of weakly deformed garnet lherzolites 141-12, 144-9 and 150-4 are less than 3%. With increasing deformation intensity and olivine contents, the P- and S-wave velocities and anisotropy gradually increase in samples 166-7, 151-11 and 160-9. According to EBSD-determined modal composition,

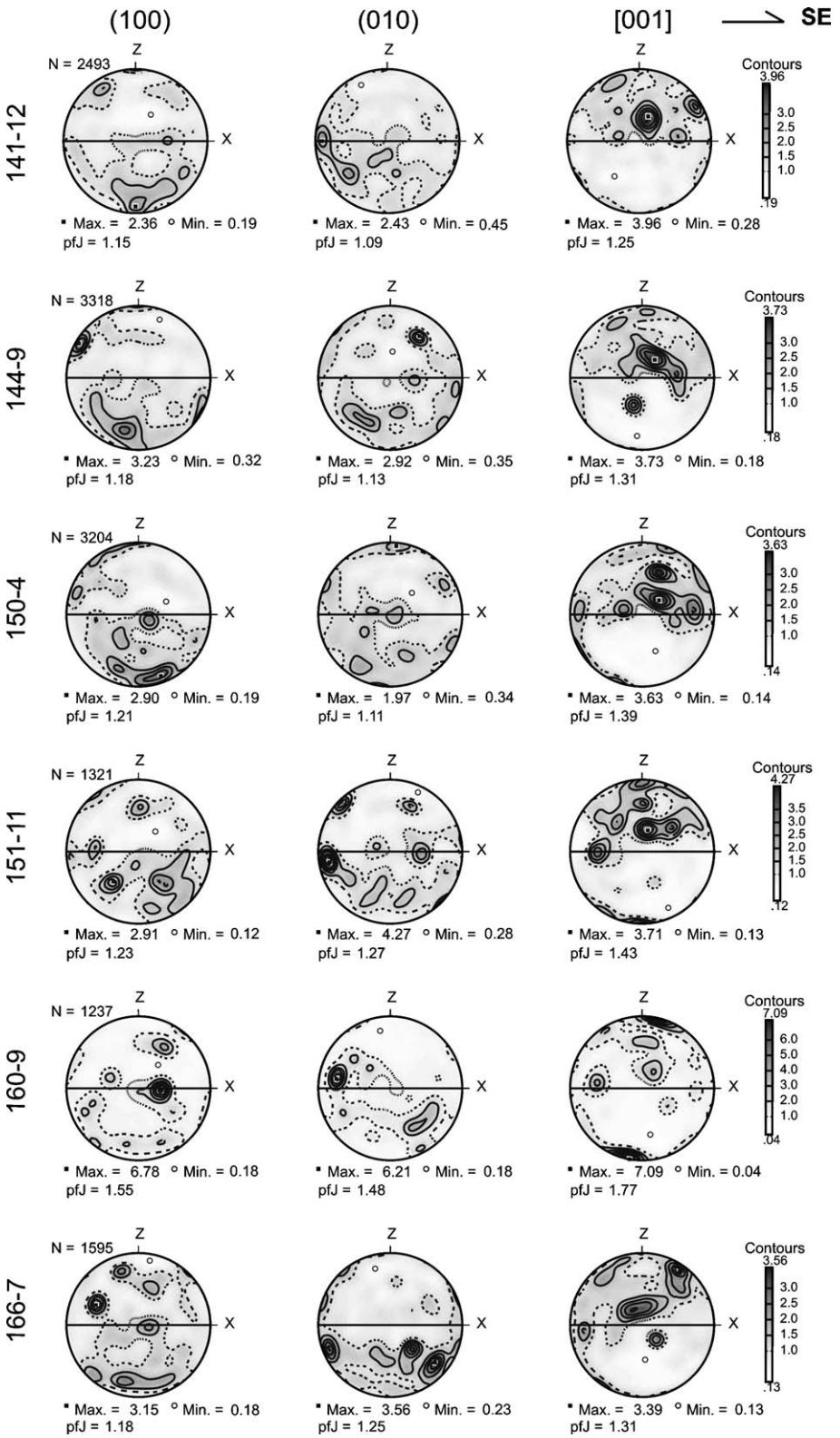

Fig. 5. EBSD-measured diopside LPO from the Zhimafang garnet peridotite. Equal area projection, lower hemisphere, contouring at multiples of a uniform distribution and an inverse log grey scale. Structural directions *X*, *Y* and *Z* are defined in the text. *N*: number of data points; pfJ: texture index.

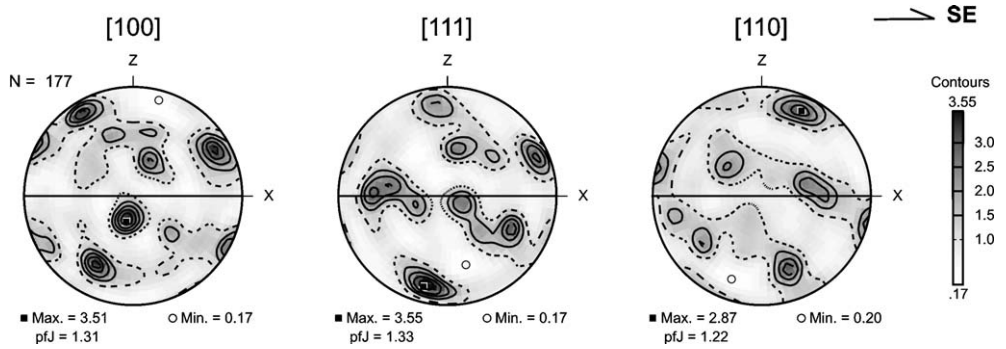

Fig. 6. Garnet LPO of the Zhimafang garnet lherzolite 144-9. Equal area projection, lower hemisphere, contouring as multiples of a uniform distribution and an inverse log grey scale. *N*: number of data points; pfJ: texture index.

the strongly foliated garnet lherzolite 160-9 yields the fastest P-wave velocity of 8.73 km/s and the largest P-wave anisotropy of 8%. If assuming all serpentine to be olivine in sample 160-9, a mixture of 75% olivine, 20% diopside and 5% enstatite would result in the fastest P-wave velocity of 8.79 km/s and the anisotropy of 8.8%. Because the fastest P-wave velocity is along the [100] axis in olivine crystal, the consistent P-wave velocity pattern indicates the significant contribution of olivine (100) [001] fabric. The fast S-wave velocities (Vs1) display complex patterns, with the slowest directions are in the foliation plane and close to the Y-direction. The largest S-wave polarization anisotropy (or the shear wave splitting) occurs subparallel to the lineation and the lowest subnormal to the foliation. The shear wave splitting ranges from 0.08 km/s to 0.27 km/s, with the largest value in foliated lherzolite 160-9. In general, the Vs1 polarization direction is normal to the foliation.

It is noteworthy that the above calculations represent the seismic properties of crack-free samples at room *P–T* conditions. The calculated velocities can yield good approximation to the measured values of peridotites at 500–600 MPa and room temperature where most microcracks are closed (Ji et al., 2003), and will increase very slowly with depth in the upper mantle because positive pressure derivatives and negative temperature derivatives of velocities essentially counteract each other (e.g., Kern and Tubia, 1993). At high pressure the anisotropy of most rocks will approach a constant and apparently is not much affected by temperature (e.g., Kern et al., 2001; Ji et al., 2002), which allows extrapolation of calculated anisotropy to greater depths. If samples contain more garnet, seismic velocity will increase but anisotropy will decrease. Christensen (2000) proposed that due to in situ variations of foliation, the overall anisotropy of a large peridotite body can be significantly lower than the anisotropy of hand samples. Therefore the anisotropy of garnet peridotite in a subducting continental slab would be difficult to detect using seismic techniques. For the garnet peridotite with a horizontal foliation, vertically propagating shear waves (e.g., SKS) would not observe any seismic anisotropy because the polarization anisotropy of shear waves is close to zero along the *Z* direction.

Table 2
Modal compositions (vol.%) of the core samples from the Zhimafang peridotite

Sample	Olivine	Diopside	Enstatite	Garnet
141-12	55	40		5
144-9	42	35	13	10
150-4	45	36	12	7
151-11	70	18	7	5
160-9	67	26	7	
166-7	65	30	3	2

6. Water content in olivine

To examine whether the (100) [001] olivine LPO in the Zhimafang garnet peridotite was formed at high water fugacity, we determine the hydroxyl concentration in olivine using Fourier transform infrared (FTIR) spectroscopy. For each sample, a polished thin section of ~0.3 mm thick was prepared and dried in an oven at 120 °C for 4 h. The infrared spectrum was obtained on Nicolet Magna-IR 750 spectrometer at room temperature and in the wave number range of 2900–4000 cm^{-1}. The measurements were carried out using an unpolarized light source, a KBr beam-splitter and a MCT detector. A series of 128 scans was averaged for each spectrum with a resolution of 8 cm^{-1}. Crack-free and unaltered regions of 10 μm in diameter were carefully selected.

Fig. 8 shows typical unpolarized FTIR spectra of olivine from the Zhimafang garnet peridotite. The

absorption bands in the range of 3400–3570 cm^{-1} present structural hydroxyl species in olivine, while peaks near 3690 cm^{-1} and 3645 cm^{-1} correspond to the OH stretching bands of serpentine, the absorption band at 3677 cm^{-1} is associated with talc, and a broad absorption near 3420 cm^{-1} may reflect submicroscopic fluid inclusions in olivine (e.g., Miller et al., 1987; Kohlstedt et al., 1996; Khisina et al., 2001). The characteristic peak of serpentine at 3687 cm^{-1} and 3640 cm^{-1} is very common in our samples, especially in partially serpentinized samples, which can be attributed to serpentine along microcracks in olivine. Only the spectra with the dominant peak near 3570 cm^{-1} are selected for the calculation of water contents.

Both the measurements and the calibration methods have significant influence on the determination of water contents. Based on the spectra of water in glasses and quartz, Paterson (1982) proposed a generic calibration to estimate water contents and introduced an orientation factor γ to approximate the full 3D absorption intensity in a single crystal:

$$c = \int \frac{K(v)}{150\gamma(3780 - v)} \mathrm{d}v \quad (1)$$

where c is the molar concentration of hydroxyl in mol H/l, $K(v)$ is the absorption coefficient in cm^{-1} at wave number v in cm^{-1}, $\gamma = 1/3$ for isotropic OH orientation distribution. The range of integration is usually from 3150 to 3750 cm^{-1}. The Zhimafang olivine is chemically homogeneous with a composition of $(Mg_{0.92}Fe_{0.08})_2SiO_4$ (Table 4). Thus the value of c should be multiplied by a factor of 4.38×10^4 or 2.70×10^3 to obtain the water content in H/10^6 Si or ppm of H_2O, respectively. The accuracy of water contents derived from Eq. (1) is in the range of 30–50%. The uncertainty comes from the use of unpolarized radiation and the orientation factor, the thickness of thin sections and the choice of baseline.

Table 5 lists the water contents in olivine, calculated by Paterson (1982) calibration. The hydroxyl concentrations in olivine from the Zhimafang garnet peridotite vary greatly, but all the values larger than 500 H/10^6 Si are from spectra with characteristic absorption bands of serpentine minerals at 3687 and 3640 cm^{-1} (Table 5), suggesting the effects of hydrothermal alteration during later exhumation. For inclusion- and fracture-free olivine crystals, the hydroxyl concentrations range from 144 to 475 H/10^6 Si, falling in the range of dry to modest water content in the olivine fabric diagram as function of water content and stress (Jung and Karato, 2001; Katayama et al., 2004). The hydroxyl concentrations of olivine grains are far below the hydroxyl solubility of olivine in the upper mantle conditions (Kohlstedt et al., 1996), implying that neither a free hydrous phase existed during UHP metamorphism nor a significant release of dissolved hydroxyl took place during exhumation.

In addition, the possibility of diffusive loss of water is very important to evaluate the measured hydroxyl concentration in olivine. For example, at least 40% hydrogen loss can be observed in olivine from mantle xenoliths (Peslier and Luhr, 2006). The Zhimafang garnet peridotite experienced the UHP metamorphism at 221±3 Ma (Zhang et al., 2005), and the later regional amphibolite–facies retrograde metamorphism at 211±4 Ma (Liu et al., 2004). The order of magnitude of diffusional transfer of hydrogen can be estimated by the diffusional length scale:

$$l = \sqrt{tD} \quad (2)$$

where t is the time scale and D is diffusion coefficient of hydrogen in olivine. According to the Arrhenius relation, the relatively low temperature of the Zhimafang peridotite will result in much lower hydrogen diffusivity in olivine. For near-isothermal decompression during the early exhumation stage, assuming t equals 10 Ma and D is 10^{-13} to 10^{-14} m^2/s at 700–800 °C in olivine (Demouchy and Mackwell, 2003; Regenauer-Lieb and Kohl, 2003), the calculated diffusional length l from water-rich olivine to dry olivine equals 2–6 m, which is much less than the size of the Zhimafang garnet peridotite body. Considering the widespread lack of penetrative aqueous fluid phases during UHP and retrograde metamorphism in the Sulu

Table 3
Calculated seismic properties and densities for the core samples from the Zhimafang garnet peridotite at ambient conditions

Sample	Density (g/cm^3)	Vp_{max} (km/s)	Vp_{min} (km/s)	A(Vp) (%)	$Vs1_{max}$ (km/s)	$Vs1_{min}$ (km/s)	A(Vs1) (%)	$Vs2_{max}$ (km/s)	$Vs2_{min}$ (km/s)	A(Vs2) (%)	A(Vs) (%)	$(Vs1-Vs2)_{max}$ (km/s)
141-12	3.37	8.41	8.18	2.80	4.86	4.79	1.50	4.81	4.73	1.60	2.63	0.13
144-9	3.38	8.40	8.20	2.40	4.84	4.81	0.60	4.83	4.75	1.50	1.81	0.09
150-4	3.37	8.40	8.20	2.30	4.85	4.81	0.80	4.82	4.75	1.40	1.58	0.08
151-11	3.37	8.56	8.09	5.70	4.93	4.79	2.80	4.84	4.70	2.90	4.30	0.21
160-9	3.34	8.73	8.07	8.00	4.99	4.77	4.30	4.84	4.63	4.50	5.50	0.27
166-7	3.35	8.49	8.07	5.10	4.92	4.78	2.80	4.81	4.70	2.20	3.94	0.19

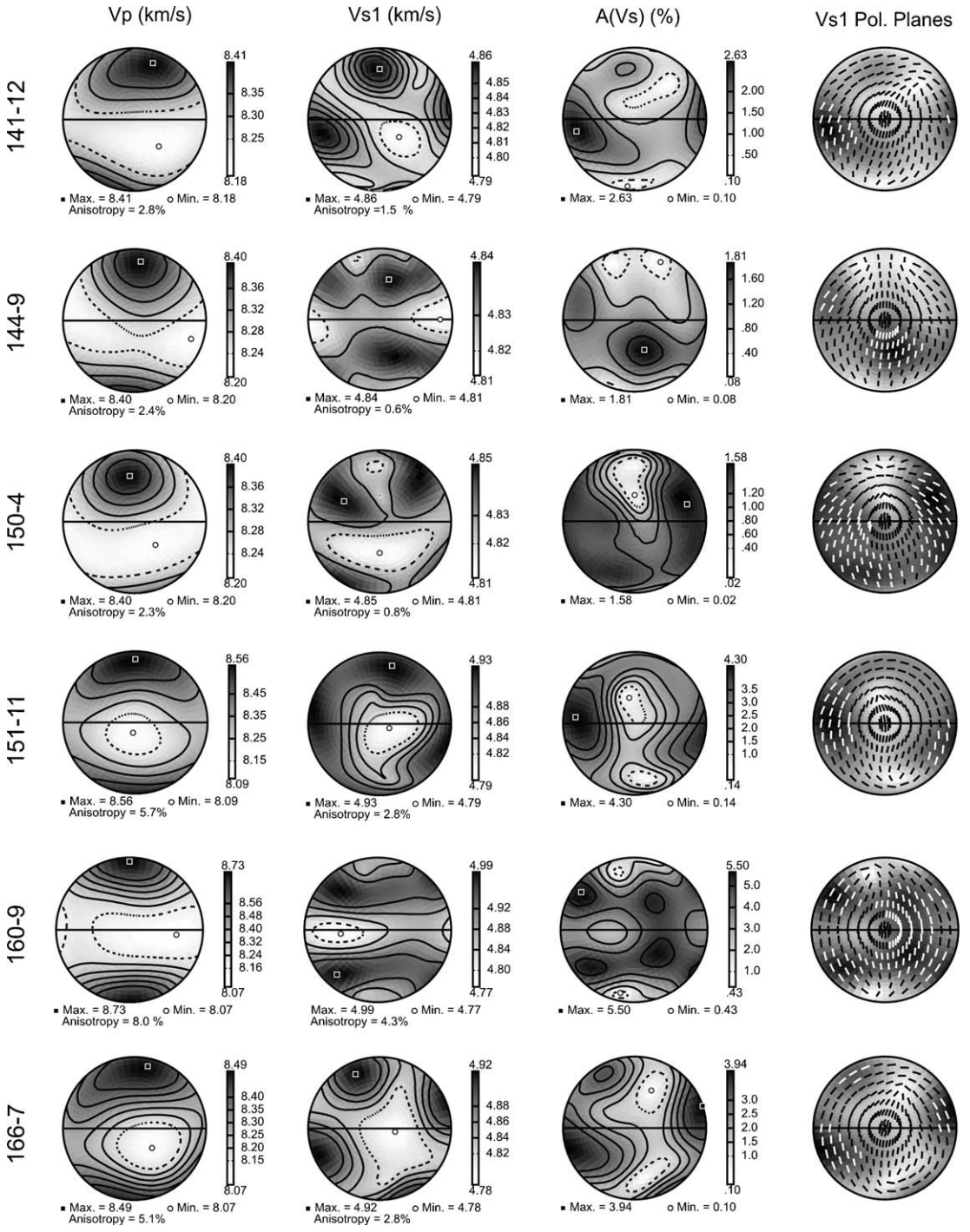

Fig. 7. Calculated P- and S-wave seismic properties of the Zhimafang garnet peridotite. A(Vs) is the shear wave polarization anisotropy. Equal area projection, lower hemisphere. Structural directions *X*, *Y* and *Z* are defined in the text.

terrane (Zheng et al., 2003), which is also supported by the common occurrence of highly localized and fine-scale retrograded metamorphic reactions, the diffusivity of hydrogen in olivine would be very low in space and geological time scale and could not significantly change the water contents in fresh olivine grains. Therefore owing to the low temperature and rapid exhumation rate, our results give the first-order estimates of water originally preserved in olivines in the UHP garnet peridotite, and infer that the dominant (100) [001] slip in olivines in the

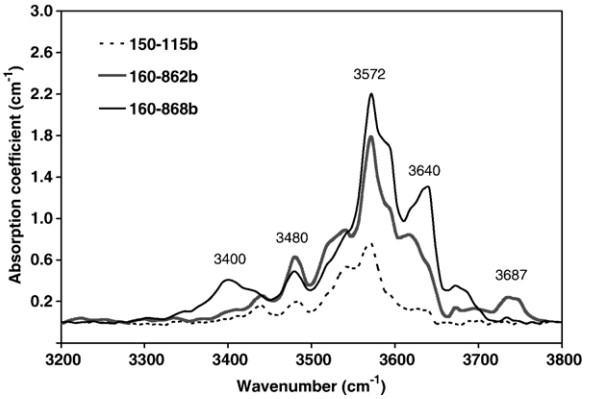

Fig. 8. Typical unpolarized FTIR spectra for studied olivine, labeling the wave numbers for absorption peaks.

Zhimafang garnet peridotite is not produced by high water contents.

Although Paterson (1982) calibration has been widely used to determine the water contents (Kohlstedt et al., 1996; Jung and Karato, 2001; Katayama et al., 2004), Bell et al. (2003) argued its reliability and proposed a new quantitative calibration for OH concentrations in olivine using polarized light along *a*, *b*, and *c* axes of olivine:

$$C_{H_2O} = 0.188 \times \mathrm{Abs}_{tot} = 0.188 \times \left(\int K_a(\nu)\mathrm{d}\nu + \int K_b(\nu)\mathrm{d}\nu + \int K_c(\nu)\mathrm{d}\nu \right) \quad (3)$$

where C_{H_2O} is water content in ppm by weight, Abs_{tot} is a total integral absorbance, $K_a(\nu)$, $K_b(\nu)$ and $K_c(\nu)$ are the absorption coefficients in cm^{-1} along *a*-, *b*-, and *c*-axes of olivine, respectively. The average OH concentrations determined from Eq. (3) are ~3.5 times the values obtained by the Paterson's calibration for the unpolarized IR spectrum with the beam parallel to [010] and $\gamma = 0.5$ (Bell et al., 2003). Unfortunately, for

Table 5
Water contents in olivine from the Zhimafang garnet peridotite

Sample	Run #	Integrated wave number (cm^{-1})	Paterson (1982) calibration		Bell et al. (2003) calibration
			C_{OH} ($H/10^6$ Si)	C_{H_2O} (wt. ppm)	C_{H_2O} (wt. ppm)
141-12	6BC[a]	3150–3660	985	61	126
150-4	y114b	3150–3750	414	26	58
	y115b	3150–3750	221	14	32
	y117b	3150–3750	393	24	55
	y118b	3150–3750	191	12	26
	y119b	3150–3750	264	16	37
	y120b	3150–3750	144	9	20
	y121b	3150–3750	475	29	65
151-11	2BC	3150–3660	442	27	62
	3BC[a]	3150–3660	504	31	72
	6BC[a]	3150–3660	1166	72	146
	10BC	3150–3660	685	42	101
160-9	y857b[a]	3150–3750	526	32	47
	y862b[a]	3150–3750	886	55	102
	y864b[a]	3150–3750	1093	68	122
	y868b[a]	3150–3750	1063	66	133
161-3	BC[a]	3368–3660	918	57	115
	3BC[a]	3368–3660	993	61	126
	4BC[a]	3368–3660	627	39	83
	6BC[a]	3368–3660	1068	66	132
	7BC[a]	3368–3660	642	40	84
	8BC[a]	3368–3661	525	32	65

[a] Absorption peaks of serpentine near 3687 and 3640 cm^{-1} were observed as the second strongest bands in olivine IR spectra, showing the occurrence of serpentine in the inclusions or crack-related alteration.

Table 4
Chemical compositions of olivine grains in the core samples from the Zhimafang garnet peridotite

Oxide (wt.%)	141-12				151-11			160-9		
Run #	#1	#2	#3	#4	#5	#6	#7	#8	#9	#10
SiO_2	41.387	41.495	41.337	41.245	41.476	41.761	41.537	41.675	41.531	41.462
TiO_2	0.015	0.046	0.017		0.049		0.014	0.036	0.047	0.017
Cr_2O_3	0.008	0.032	0.015				0.026	0.010		
MgO	49.362	49.450	49.031	49.510	49.276	49.916	49.905	49.985	49.297	50.074
CaO	0.005	0.001	0.003			0.010	0.001			
MnO	0.085	0.062	0.100	0.033	0.145	0.051	0.084	0.072	0.048	0.013
FeO	8.554	8.344	8.497	8.386	7.764	8.046	8.018	7.992	8.068	8.158
NiO	0.451	0.378	0.418	0.387	0.433	0.401	0.405	0.355	0.335	0.364
Na_2O		0.014	0.030		0.021	0.002		0.006	0.019	0.011
K_2O	0.033	0.024	0.020	0.053		0.030	0.036	0.037	0.046	0.047
Total	99.901	99.847	99.468	99.615	99.164	100.217	100.025	100.168	99.391	100.145
fo (mol%)	91.06	91.29	91.05	91.29	91.74	91.67	91.65	91.70	91.54	91.61
fa (mol%)	8.85	8.64	8.85	8.68	8.11	8.29	8.26	8.23	8.41	8.37

fo: forsterite; fa: fayalite

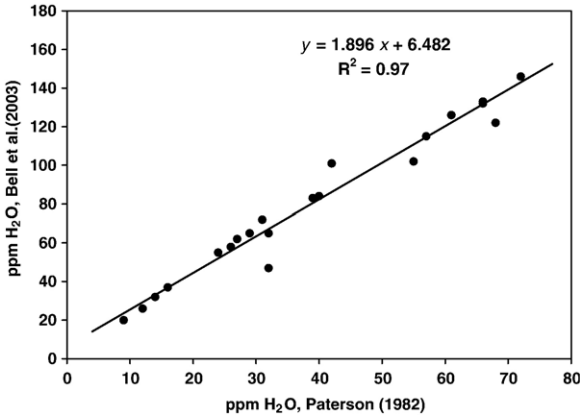

Fig. 9. Comparison of olivine water contents determined using Bell et al. (2003) and Paterson (1982) calibration methods for unpolarized FTIR spectra and randomly oriented olivine crystals.

randomly oriented crystals, they did not give experimental verification. Assuming the total integral absorbance Abs_{tot} could be approximated by $3\times\int K(\nu)d\nu$ from one orientation, we applied Eq. (3) to estimate the water contents in olivine (Table 5). It is interesting to notice that the water contents obtained from the calibration of Bell et al. (2003) are ~1.9 times the values derived from the Paterson (1982) method (Fig. 9). This provides a possibility to compare water contents calculated from two methods for the unpolarized case and randomly oriented olivine crystals.

7. Olivine deformation mechanism in the subducted continental slab

Detailed geochronology and geochemistry studies demonstrate that the Zhimafang garnet peridotite was captured from a mantle wedge immediately adjacent the subducted Yangtze slab and then experienced the UHP metamorphism at 750–950 °C and 4–7 GPa with extremely low geothermal gradient (≤5 °C/km) (Zhang et al., 1994, 2000; Yang and Jahn, 2000). A top-to-NW thrusting has been documented from the exhumation-induced quartz LPOs in paragneiss and granitic gneiss (Xu et al., 2003b), which is in contrary with the top-to-SE shear sense inferred from the olivine LPO pattern (Fig. 3). Once formed, the LPO is difficult to be modified during later annealing (Heilbronner and Tullis, 2002). Therefore, the opposite shear senses between olivine and quartz reflect different deformation stages of the Sulu UHP rocks. The (100) [001] olivine fabrics of the Zhimafang garnet peridotite most likely record the peak UHP metamorphism and were preserved during late exhumation.

The (100) [001] slip system has been reported in olivine from chondrites (Carter et al., 1968), in the garnet peridotites from Alpe Arami (Möckel, 1969) and Cima di Gagnone (Frese et al., 2003) in the Central Alps and the Norwegian Caledonides (Katayama et al., 2005). The Alpe Arami peridotite was derived from a subcontinental mantle (Pfiffner and Trommsdorff, 1998), and the Cima di Gagnone peridotite from a partially serpentinized mantle beneath a pre-Alpine ocean near a continental margin (Evans et al., 1979; 1981). These rocks were subducted during Alpine orogeny in a hydrous subduction slab (Frese et al., 2003) with peak metamorphic conditions of 3.0–3.2 GPa and 750–840 °C (Nimis and Trommsdorff, 2001). However, the isotopic values of the Zhimafang peridotite indicate that the crustal fluid–rock interaction was very limited (Li et al., 2003a,b). Compared with subduction of oceanic lithosphere, the subduction of old, cold and dry continental materials of the Yangtze plate provided a fluid-deficient environment, where most volatile and fluids have been stored in HP and UHP hydrous minerals (Liou et al., 1998). The unusually low $\alpha^{18}O$ values preserved in the Dabie–Sulu UHP rocks confirm the absence of pervasive fluid infiltration during both earlier prograde, peak UHP metamorphism and later retrograde metamorphism (Zheng et al., 2003). Hence the deformation conditions of the Zhimafang garnet peridotite are characterized by ultrahigh pressure, low temperature and low water fugacity.

In experiments of Jung and Karato (2001), the water-induced (100) [001] olivine fabric formed at pressure of ~2 GPa and temperature of 1200–1300 °C. The results obtained from their experimental conditions do not seem to be applicable to explain the origin of olivine LPOs in the Zhimafang garnet peridotite. Recent experiments

have highlighted the role of UHP in the formation of (100) [001] olivine fabrics. Raterron et al. (2004) reported the high density of '*c*'-dislocations in dry (water content <1 ppm) olivine deformed at high pressures up to 9 GPa and temperatures lower than 890 °C, which are comparable with the P–T conditions in a subducted slab. The activation of {110}[001] slip systems was also found in dry (water content <1 ppm) olivine deformed at a pressure of 8 GPa and temperatures of 700–1000 °C. At 1000 °C, although the '*c*'-dislocation glide is still dominant, [100] glide dislocations are equally observed, implying the temperature-dependent transition of olivine fabric at high pressures. Couvy et al. (2004) summarized the critical resolved shear stress of (010) [100] and (010) [001] as a function of temperature and demonstrated that the development of [001] glide is easier than [100] glide at temperature lower than 900 °C. However, in shear deformation experiments at 11 GPa and 1400 °C, the olivine LPO pattern is still characterized by (100) [001] and sometimes (010)[001] slip systems, suggesting a pressure-induced modification of dislocation core structure (Couvy et al., 2004). The high-pressure-induced [001] systems have been confirmed by simulation using a viscoplastic self-consistent model (Mainprice et al., 2005). Therefore, UHP is indeed an important factor to promote (100) [001] slip system in olivine. The olivine fabrics observed in the Zhimafang garnet peridotite was formed by dominant (100) [001] slip under the peak metamorphic conditions at UHP, low temperature and relatively low water content.

8. Conclusions

Lattice preferred orientations (LPOs) of olivine, diopside, enstatite and garnet from the Zhimafang garnet peridotite were quantitatively studied using EBSD technique. In all studies samples, olivine developed strong LPOs characterized by the concentration of [001] axes subparallel with the lineation, and the [100] axes are roughly normal to the foliation. Diopside developed complex LPO patterns that are difficult to explain using a single slip system as usually done for those fabrics observed in the lower crustal mafic mylonites (Ji et al., 1993) and ophiolitic peridotites (Nicolas and Poirier, 1976). Enstatite LPOs can be reasonably explained by the dominance of (100) [001] slip. Garnet is almost randomly orientated due to its low volume fractions, cubic symmetry and the presence of numerous slip systems. The strong LPOs demonstrate that dislocation creep is the dominant deformation mechanism for olivine in the UHP garnet peridotite. The calculated fast P-wave velocities are normal to the foliation, with values from 8.40 to 8.73 km/s. The P-wave anisotropy varies from 2.4% to 8% and its pattern is mainly controlled by olivine (100) [001] slip system. The maximum shear wave anisotropy (or shear wave splitting) appears subparallel to the foliation and the Vs1 polarization plane is generally normal to the foliation.

The top-to-SE shear sense inferred from the asymmetry of olivine LPO with respect to the structural foliation and lineation is different from the exhumation-induced top-to-NW thrusting determined from the quartz LPO in the study region. This fact suggests that the olivine LPOs preserved in the Zhimafang peridotite provide a record of the earlier UHP metamorphism. Water contents in fresh and inclusion-free olivine crystals (141–475 H/10^6 Si), which were determined using Fourier transform infrared (FTIR) spectroscopy and Paterson (1982) calibration, are much lower than those required to develop (100) [001] slip system in experiments of Jung and Karato (2001). Although water may enhance, to some extent, the slip along the [001] direction, clearly it is not the principal controlling factor in the case of the Zhimafang peridotite. Considering the *P–T* conditions of the peridotite and recent experiments in olivine rheology at higher confining pressures, we conclude that the olivine (100) [001] slip system of the Zhimafang garnet peridotite was prevailing under the conditions of high pressure, low temperature and low water content during the subduction of cold and dry supracrustal rocks of the Yangtze plate.

Acknowledgements

The EBSD measurements were carried out in the Key Laboratory of Continental Dynamics, Chinese Ministry of Land and Resources. Prof. L.H. Guo helped in the water content measurements. We are grateful to Dr. D. Mainprice and another reviewer for their constructive suggestions. This research is funded by the Chinese Ministry of Science and Technology (2003CB716504), the Natural Science Foundation of China (40399143), and the Chinese Ministry of Land and Resources (2002207).

References

Abramson, E.H., Brown, J.M., Slutsky, L.J., Zang, J., 1997. The elastic constants of San Carlos olivine to 17 GPa. J. Geophys. Res. 102, 12253–12263.

Bell, D.R., Rossman, G..R., Maldener, J., Endisch, D., Rauch, F., 2003. Hydroxide in olivine: a quantitative determination of the

absolute amount and calibration of the IR spectrum. J. Geophys. Res. 108 (B2), 2105, doi:10.1029/2001JB000679.
Ben Ismaïl, W., Mainprice, D., 1998. An olivine fabric database: an overview of upper mantle fabrics and seismic anisotropy. Tectonophysics 269, 145–157.
Brueckner, H.K., Medaris, L.G., 2000. A general model for the intrusion and evolution of 'mantle' peridotite in high-pressure and ultrahigh-pressure metamorphic terranes. J. Metamorph. Geol. 18, 123–133.
Carter, N.L., Avé Lallemant, H.G., 1970. High temperature flow of dunite and peridotite. Geol. Soc. Amer. Bull. 81, 2181–2202.
Carter, N.L., Raleigh, C.B., Decarli, P.S., 1968. Deformation of olivine in stony meteorites. J. Geophys. Res. 73, 5439–5461.
Chai, M., Brown, J.M., Slutsky, L.J., 1997a. The elastic constants of an aluminous orthopyroxene to 12.5 GPa. J. Geophys. Res. 102, 14779–14785.
Chai, M., Brown, J.M., Slutsky, L.J., 1997b. The elastic constants of pyrope–grossuar–almandine garnet to 20 GPa. Geophys. Res. Lett. 24, 523–526.
Christensen, N.I., 2000. Continental mantle seismic anisotropy: a new look at the Twin Sisters massif. Tectonophysics 355, 163–170.
Collins, M.D., Brown, J.M., 1998. Elasticity of an upper mantle clinopyroxene. Phys. Chem. Miner. 26, 7–13.
Couvy, H., Frost, D.J., Heidelbach, F., Nyilas, K., Ungar, T., Mackwell, S., Cordier, P., 2004. Shear deformation experiments of forsterite at 11 GPa–1400 °C in the multianvil apparatus. Eur. J. Mineral. 16, 877–889.
Demouchy, S., Mackwell, S., 2003. Water diffusion in synthetic iron-free forsterite. Phys. Chem. Miner. 30, 486–494.
Evans, B.W., Trommsdorff, V., Richter, W., 1979. Petrology of an eclogite–metarodingite suite at Cima di Gagnone, Ticino, Switzerland. Am. Mineral. 64, 15–31.
Evans, B.W., Trommsdorff, V., Goles, G.G., 1981. Geochemistry of high-grade eclogites and metarodingites from the Central Alps. Contrib. Mineral. Petrol. 76, 301–311.
Faure, M., Lin, W., Monié, P., Le Breton, N., Poussineau, S., Panis, D., Etienne, D., 2003. Exhumation tectonics of the ultrahigh-pressure metamorphic rocks in the Qinling orogen in East China: new petrological–structural–radiometric insights from the Shandong Peninsula. Tectonics 22, doi:10.1029/2002TC001450.
Frese, K., Trommsdorf, V., Kunze, K., 2003. Olivine [100] normal to foliation: lattice preferred orientation in prograde garnet peridotite formed at high H_2O activity, Cima di Gagnone (Central Alps). Contrib. Mineral. Petrol. 145, 73–86.
Hacker, B.R., Ratschbacher, L., Webb, L.E., McWilliams, M.O., Ireland, T., Calvert, A., Dong, S.W., Wenk, H.R., Chateigner, D., 2000. Exhumation of ultrahigh-pressure continental crust in east central China: late triassic–early Jurassic tectonic unroofing. J. Geophys. Res. 105, 13,339–13,364.
Heilbronner, R., Tullis, J., 2002. The effect of strain annealing on microstructure and crystallographic preferred orientations of quartzites experimentally deformed in axial compression and shear. In: De Meer, S., et al. (Ed.), Deformation Mechanisms, Rheology and Tectonics: Current Status and Future Perspectives. Geological Society of London, pp. 191–218.
Ji, S., Salisbury, M.H., Hanmer, S., 1993. Petrofabric, P-wave anisotropy and seismic reflectivity of high-grade tectonites. Tectonophysics 222, 195–226.
Ji, S., Zhao, X., Francis, D., 1994. Calibration of shear-wave splitting in subcontinental upper mantle beneath active orogenic belts using ultramafic xenoliths from the Canadian Cordillera and Alaska. Tectonophysics 239, 1–28.
Ji, S.C., Wang, Q., Xia, B., 2002. Handbook of Seismic Properties of Minerals, Rocks and Ores. Polytechnic International Press, Montreal, Canada. 630 pp.
Ji, S., Saruwatari, K., Mainprice, D., Wirch, R., Xu, Z.Q., Xia, B., 2003a. Microstructures, petrofabrics and seismic properties of ultrahigh-pressure eclogites from Sulu region, China: implications for rheology of subducted continental crust and origin of mantle reflections. Tectonophysics 370, 49–76.
Ji, S.C., Wang, Q., Xia, B., 2003b. P-wave velocities of polymineralic rocks: comparison of theory and experiment and test of elastic mixture rules. Tectonophysics 366, 165–185.
Jung, H., Karato, S., 2001. Water-induced fabric transitions in olivine. Science 293, 1460–1463.
Katayama, I., Jung, H., Karato, S., 2004. New type of olivine fabric from deformation experiments at modest water content and low stress. Geology 32, 1045–1048.
Katayama, I., Karato, S., Brandon, M., 2005. Evidence of high water content in the deep upper mantle inferred from deformation microstructures. Geology 33, 613–616.
Kern, H., Tubia, J.M., 1993. Pressure and temperature dependence of P- and S-wave velocities, seismic anisotropy and density of sheared rocks from Sierra Alpujata massif (Ronda peridotites, southern Spain). Earth Planet. Sci. Lett. 119, 191–205.
Kern, H., Popp, T., Gorbatsevich, F., Zharikov, A., Lobanov, K.V., Smirnov, Yu.P., 2001. Pressure and temperature dependence of Vp and Vs in rocks from the superdeep well and from surface analogues at Kola and the nature of velocity anisotropy. Tectonophysics 338, 113–134.
Khisina, N.R., Wirth, R., Andrut, M., Ukhanov, A.V., 2001. Extrinsic and intrinsic modes of hydrogen occurrence in natural olivine: FTIR and TEM investigation. Phys. Chem. Miner. 28, 291–301.
Kohlstedt, D.L., Keppler, H., Rubie, D.C., 1996. Solubility of water in the phases of $(Mg,Fe)_2SiO_4$. Contrib. Mineral. Petrol. 123, 345–357.
Krieger Lassen, N.C., 1996. The relative precision of crystal orientations measured from electron backscattering patterns. J. Microsc. 181, 72–81.
Li, S.G., Jagoutz, E., Lo, C., Chen, Y., Li, Q., Xiao, Y., 1999. Sm/Nd, Rb/Sr, and $^{40}Ar/^{39}Ar$ isotopic systematics of the ultrahigh-pressure metamorphic rocks in the Dabie–Sulu Belt, central China: a retrospective view. Int. Geol. Rev. 41, 1114–1124.
Li, L., Raterson, P., Weidner, D., Chen, J., 2003a. Olivine flow mechanism at 8 GPa. Phys. Earth Planet. Inter. 138, 113–129.
Li, T.F., Yang, J.S., Zhang, R.Y., 2003b. Peridotite from the pre-pilot hole (PP1) of the Chinese Continental Scientific Drilling Project and its bearing on depleted and metasomatic upper mantle. Acta Geol. Sin. 77, 492–509.
Liou, J.G., Zhang, R.Y., Ernst, W.G., Rumble, D., Shigenori, M., 1998. High-pressure minerals from deeply subducted metamorphic rocks. Rev. Miner. 37, 33–96.
Liou, J.G., Hacker, B.R., Zhang, R.Y., 2000a. Into the forbidden zone. Science 287, 1215–1216.
Liou, J.G., Zhang, R.Y., Jahn, B.-M., 2000b. Petrological and geochemical characteristics of ultrahigh-pressure metamorphic rocks from the Dabie–Sulu terrane, east-central China. Int. Geol. Rev. 42, 328–352.
Liu, F.L., Xu, Z.Q., Katayama, I., Yang, J.S., Maruyama, S., Liou, J.G., 2001. Mineral inclusions in zircons of para- and orthogneiss from pre-pilot drillhole CCSD-PP1, Chinese Continental Scientific Drilling project. Lithos 59, 199–215.

Liu, F.L., Xu, Z.Q., Liou, J.G., Katayama, I., Massago, H., Maruyama, S., Yang, J.S., 2002. Ultrahigh-pressure mineral inclusions in zircons from gneissic core samples of the Chinese Continental Scientific Drilling site in eastern China. Eur. J. Mineral. 14, 499–512.

Liu, F.L., Xu, Z.Q., Liou, J.G., Song, B., 2004. SHRIMP U–Pb ages of ultrahigh-pressure and retrograde metamorphism of gneisses, south-western Sulu terrane, eastern China. J. Metamorph. Geol. 22, 315–326.

Mainprice, D., 1990. A Fortran program to calculate seismic anisotropy from the lattice preferred orientation of minerals. Comput. Geosci. 16, 385–393.

Mainprice, D., 2005. The UNICEF Careware software package. http://www.isteem.univ-montp2.fr/TECTONOPHY/petrophysics/software/petrophysics_software.html.

Mainprice, D., Silver, P.G., 1993. Interpretation of SKS-waves using samples from the subcontinental lithosphere. Phys. Earth Planet. Inter. 78, 257–280.

Mainprice, D., Bascou, J., Cordier, P., Tommasi, A., 2004. Crystal preferred orientations of garnet: comparison between numerical simulations and electron back-scattered diffraction (EBSD) measurements in naturally deformed eclogites. J. Struct. Geol. 26, 2089–2102.

Mainprice, D., Tommasi, A., Couvy, H., Cordier, P., Frost, D.J., 2005. Pressure sensitivity of olivine slip systems and seismic anisotropy of Earth's upper mantle. Nature 433, 731–733.

Medaris, L.G., 1999. Garnet peridotite in Eurasian HP and UHP terranes: a diversity of origin and thermal histories. Int. Geol. Rev. 41, 799–815.

Mercier, J.-C.C., 1985. Olivine and pyroxenes. In: Wenk, H.-R. (Ed.), Preferred Orientation in Deformed Metals and Rocks: An Introduction to Modern Texture Analysis. Academic Press, pp. 407–430.

Miller, G.H., Rossman, G.R., Harlow, G.E., 1987. The natural occurrence of hydroxide in olivine. Phys. Chem. Miner. 14, 461–472.

Mizukami, T., Wallis, S.R., Yamamoto, J., 2004. Natural examples of olivine lattice preferred orientation patterns with a flow-normal *a*-axis maximum. Nature 427, 432–436.

Möckel, J.R., 1969. Structural petrology of the garnet peridotite of Alpe Arami (Ticino, Switzerland). Leidse Geol. Meded. 42, 61–130.

Nicolas, A., Christensen, N.I., 1987. Formation of anisotropy in upper mantle peridotites – a review. In: Fuchs, K., Froideoaux, C. (Eds.), Composition, Structure and Dynamics of the Lithosphere–Asthenosphere System, pp. 407–433. Trans. ed. Washington, D.C.: AGU 16.

Nicolas, A., Poirier, J.P., 1976. Crystalline Plasticity and Solid State Flow in Metamorphic Rocks. John Wiley and Sons, pp. 174–177.

Nimis, P., Trommsdorff, V., 2001. Revised thermobarometry of Alpe Arami and other garnet peridotites from the central Alps. J. Petrol. 42, 103–115.

Park, J., Levin, V., 2002. Seismic anisotropy: tracing plate dynamics in the mantle. Science 296, 485–489.

Paterson, M.S., 1982. The determination of hydroxyl by infrared absorption in quartz silicate glasses and similar materials. Bull. Miner. 105, 20–29.

Peslier, A.H., Luhr, J.F., 2006. Hydrogen loss from olivines in mantle xenoliths from Simcoe (USA) and Mexico: mafic alkalic magma ascent rates and water budget of the sub-continenal lithosphere. Earth Planet. Sci. Lett. 242, 302–319.

Pfiffner, M., Trommsdorff, V., 1998. The high-pressure ultramafic–mafic–carbonate suite of Cima Lunga–Adula, Central Alps: excursions to Cima di Gagnone and Alpe Arami. Schweiz. Mineral. Petrogr. Mitt. 78, 337–354.

Qiu, H.J., Xu, Z.Q., Zhang, Z.M., Yang, J.S., Yang, T.N., Zhang, J., Li, H.B., 2002. New mineral evidence of high-pressure metamorphism of the Subei high-pressure belt: aragonite inclusions in garnet from greenschist. Geol. Bull. China 21, 617–624.

Raterron, P., Wu, Y., Weidner, D.J., Chen, J., 2004. Low-temperature olivine rheology at high pressure. Phys. Earth Planet. Inter. 145, 149–159.

Regenauer-Lieb, K., Kohl, T., 2003. Water solubility and diffusivity in olivine: its role in planetary tectonics. Mineral. Mag. 67, 697–715.

Saruwatari, K., Ji, S., Long, C.X., Salisbury, M., 2001. Seismic anisotropy of mantle xenoliths and constraints on the upper mantle structures beneath the southern Canadian Cordillera. Tectonophysics 339, 399–422.

Savage, M.K., 1999. Seismic anisotropy and mantle deformation: what have we learned from shear wave splitting? Rev. Geophys. 37, 65–106.

Tommasi, A., Mainprice, D., Canova, G., Chastel, Y., 2000. Viscoplastic self-consistent and equilibrium-based modeling of olivine lattice preferred orientations: implications for the upper mantle seismic anisotropy. J. Geophys. Res. 105, 7893–7908.

Wenk, H.-R., Tomé, C., 1999. Modeling dynamic recrystallization of olivine aggregates deformed in simple shear. J. Geophys. Res. 104, 25513–25527.

Xu, Z.Q., Chen, J., Yang, J.S., Li, X.P., Chen, F.Y., 2003a. Discovery of titanoclinohumite and titanochondrodite exsolution in clinopyroxene included in garnet peridotite and their significance. Acta Geol. Sin. 77, 549–555.

Xu, Z.Q., Zhang, Z.M., Liu, F.L., Yang, J.S., Li, H.B., Yang, T.N., Qiu, H.J., Li, T.F., Meng, F.C., Cheng, S.Z., Tang, Z.M., Chen, F.Y., 2003b. Exhumation structure and mechanism of the Sulu ultrahigh-pressure metamorphic belt, central China. Acta Geol. Sin. 77, 433–450.

Yang, J.J., Jahn, B.-M., 2000. Deep subduction of mantle-derived garnet peridotites from the Su-Lu UHP metamorphic terrane in China. J. Metamorph. Geol. 18, 167–180.

Yang, J.J., Godard, G., Kienast, J.R., Lu, Y., Sun, J., 1993. Ultrahigh-pressure magnesite-bearing garnet peridotites from northeastern Jiangsu, China. J. Geol. 101, 541–554.

Ye, K., Yao, Y.P., Katayama, I., Cong, B., Wang, Q., Maruyama, S., 2000. Large areal extent of ultrahigh-pressure metamorphism in the Sulu ultrahigh-pressure terrane of east China: new implications from coesite and omphacite inclusions in zircon of granitic gneiss. Lithos 52, 157–164.

Zhang, R.Y., Liou, J.G., Cong, B.L., 1994. Petrogenesis of garnet-bearing ultramafic rocks and associated eclogites in the Su-Lu ultrahigh-P metamorphic terrane, eastern China. J. Metamorph. Geol. 12, 169–186.

Zhang, R.Y., Liou, J.G., Yang, J.S., Yui, T.F., 2000. Petrochemical constraints for dual origin of garnet peridotites from the Dabie–Sulu UHP terrane, eastern-central China. J. Metamorph. Geol. 18, 149–166.

Zhang, R.Y., Liou, J.G., Shu, J.F., 2002. Hydroxyl-rich topaz in high-pressure and ultrahigh-pressure kyanite quartzite with retrograde woodhouseite from the Sulu terrane, eastern China. Am. Mineral. 87, 445–453.

Zhang, R.Y., Liou, J.G., Yang, J.S., Ye, K., 2003. Ultrahigh-pressure metamorphism in the forbidden zone: the Xugou garnet peridotite, Sulu terrane, eastern China. J. Metamorph. Geol. 21, 539–550.

Zhang, R.Y., Yang, J.S., Wooden, J.L., Liou, J.G., Li, T.F., 2005. U–Pb SHRIMP geochronology of zircon in garnet peridotite from the Sulu UHP terrane, China: implications for mantle metasomatism and subduction-zone UHP metamorphism. Earth Planet. Sci. Lett. 237, 729–743.

Zheng, Y.F., Fu, B., Gong, B., Li, L., 2003. Stable isotope geochemistry of ultrahigh pressure metamorphic rocks from the Dabie–Sulu orogen in China: implications for geodynamics and fluid regime. Earth-Sci. Rev. 62, 105–161.